Enhancement of Z-scheme behavior by coupling local WO_{3-x}-WS_2 with Au nanoparticles for efficient photoelectrochemical degradation of methylene blue

Qian Guo[a], Ying Wen[a], Tian Zhang[a], Long Ren[b], Xiaohui Ren[a,*], Yang Li[a], Huanyu He[a], Huating Liu[c,*], Ye Zhang[d,*], Hua Zhang[a], Hongwei Ni[a]

[a] School of Metallurgy and Energy，Wuhan University of Science and Technology, Wuhan 430081, P. R. China

[b] Institute for Quantum Science and Technology, Shanghai University, Shanghai 200444, P. R. China

[c] School of Electrical and Electronic Engineering, Wuhan Polytechnic University, Wuhan 430023, P. R. China

[d] Lab of Optoelectronic Technology for Low Dimensional Nanomaterials, School of Chemistry and Chemical Engineering, University of South China, Hengyang 421001, P. R. China

[*] Corresponding authors: Xiaohui Ren (xhren@wust.edu.cn); Huating Liu (liuht@whpu.edu.cn); Ye Zhang (yezhang@usc.edu.cn).

Table of Contents

Table. S3 Degradation efficiency of pollutants by individual WO_3 and WS_2.

Experimental Section

Materials

Propanol (C_3H_6O, AR, 99.7%), ethanol (C_2H_5OH, AR, 99.7%), thiourea (CH_4N_2S, AR,), Methylene Blue ($C_{16}H_{18}ClN_3S \cdot 3H_2O$,), sodium oxalate ($Na_2C_2O_4$, AR, 99.8%) and anhydrous sodium sulphate (Na_2SO_4, AR, 99.0%) were purchased from Sinopharm Chemical Reagent Co. Hydrochloric acid (HCl, 36%) was purchased from Henan Kaifeng Dongda Chemical Co. Sodium citrate ($C_6H_5Na_3O_7 \cdot 2H_2O$, 99%), sodium tungstate ($Na_2WO_4 \cdot 2H_2O$, AR, 99.5%), and chloroauric acid trihydrate ($HAuCl_4 \cdot 3H_2O$, 48-50% Au-based) were purchased from Shanghai McLean Biochemistry and Technology Co. Ammonium chloride (NH_4Cl, 99.5%) was purchased from Tianjin Damao Chemical Reagent Factory. FTO conductive glass (7 Ω, transmittance≥80%) purchased from Wuhan Jingge Solar Technology Co. Hydrogen peroxide 30% aqueous solution (H_2O_2) purchased from Tianjin Tianli Chemical Reagent Co. Tungstic acid (H_2WO_4, AR) was purchased from Chemical Reagent No.2 Factory. The deionized water used in this experiment was homemade in the laboratory with a resistivity test value of 18.2 MΩ cm^{-1}.

Hydrothermal preparation of WO_{3-x}

The FTO conductive glass was first ultrasonically cleaned three times with propanol, ethanol and distilled water for 15 minutes, dried and prepared for use. 0.5 M tungstic acid and 0.5 M H_2O_2 solution were mixed and stirred for 24 h to obtain the tungstic acid seed layer. The seed layer was evenly coated on the front side of FTO conductive glass, and then heated in a muffle furnace at 450℃ for 30 minutes, and then cooled naturally and prepared for use.

Then, the precursor solution was obtained by adding 0.134 g of sodium tungstate, 0.402 g of sodium oxalate and 0.259 g of ammonium chloride to 30 ml of distilled water, stirring for 30 min, and adding concentrated hydrochloric acid droppage by froth to adjust the pH=1.

Finally, the prepared glass was placed vertically into the tetrafluoroethylene liner containing the precursor solution, and the hydrothermal temperature was controlled at

120℃, 140℃, 160℃, 180℃, and 200℃. The hydrothermal temperature was set at 120℃, 140℃, 160℃, 180℃, and 200℃. The hydrothermal time was 4 h, 8 h, 12 h and 36 h. After the hydrothermal reaction, the glass pieces were removed and cleaned and dried to obtain the FTO loaded with WO_{3-x}.

Preparation of WO_{3-x}@Au

WO_{3-x}@Au catalysts were prepared by photodeposition. Mixing 1 mL of chloroauric acid with 29 mL of sodium citrate stir it well and placed in a quartz glass reactor for spare put it into a quartz glass reactor. The glass side containing WO_3 was placed into the mixed solution by aligning the glass side with the light source, controlling the distance at about 5 cm, and photodeposition was carried out under the irradiation of UV light to obtain WO_{3-x}-Au.

Preparation of in-situ sulfurization samples

Grinding of 0.2 g of thiourea was incorporated into the porcelain boat a, the prepared FTO slant loaded with catalyst was incorporated into the porcelain boat b, and the porcelain boat 1 was placed in front of the porcelain boat b, and annealed at 450℃ under Ar atmosphere for 2 h. Catalyst loaded with WS_2 was received.

Material characterization

The phase composition and chemical state of the samples were characterized by X-ray diffraction (XRD, XPERT MPD Pro), X-ray photoelectron spectroscopy (XPS, Thermo Scientific K-Alpha) and Raman spectroscopy (Raman, Horiba LabRAM HR Evolution). The surface morphology of the samples was obtained by field emission scanning electron microscopy at 10 KV (FE-SEM, FEI Nova NANOSEM 400), TEM, HR-TEM, EDS and elemental mapping (JEM-F200). Free radical and retrograde studies of the samples during reaction were carried out using a steady state/transient fluorescence spectrometer (Edinburgh FLS1000). Detection of absorbance was carried out by a visible photometer (V-T3). Ultraviolet-visible (UV–vis) spectroscopy were recorded on a pgeneral TU-1901 Dual-beam UV-Vis spectrophotometer equipped with an integrating sphere, and $BaSO_4$ powders were used as a reflectance standard. Electrochemical measurements were carried out with a CHI660E electrochemical workstation (Shanghai Chenhua, China).

Experiments for PEC degradation

The photoelectrocatalytic activity of the prepared samples was evaluated by simulating the degradation of MB solution under visible light. In the photoelectrocatalysis experiment, a magnetic stirrer was placed at the bottom of a quartz glass reactor, the bias voltage was set to 0.7 V vs. Ag/AgCl, and the xenon lamp was adjusted to 100 mW cm^{-2}. The reactor was placed approximately 5 cm away (20 mW cm^{-2}) from the xenon lamp light source. 30 mL of 10 ppm MB solution was added to the reactor and the prepared sample was held submerged in the solution using an electrode holder. Before the start of the photoreaction, it was left for 30 minutes in dark to reach adsorption equilibrium. After the start of the photoreaction, 3 mL of the mixed solution was taken at intervals, centrifuged and the supernatant was extracted. The absorbance at 664 nm (absorption peak of MB) was determined by UV-visible photometer. The MB degradation rate was calculated as follows:

$$\eta = \frac{C_0 - C}{C_0} \times 100\% \quad (1)$$

Where: **η**-degradation rate, %;

C-The MB solution concentration for each time period, mol L^{-1};

C_0-The MB solution's initial concentration, mol L^{-1}.

The photocurrent signals were recorded without applied potential using a three-electrode system, with a Pt wire and Ag/AgCl electrode for the counter and reference electrodes, respectively.

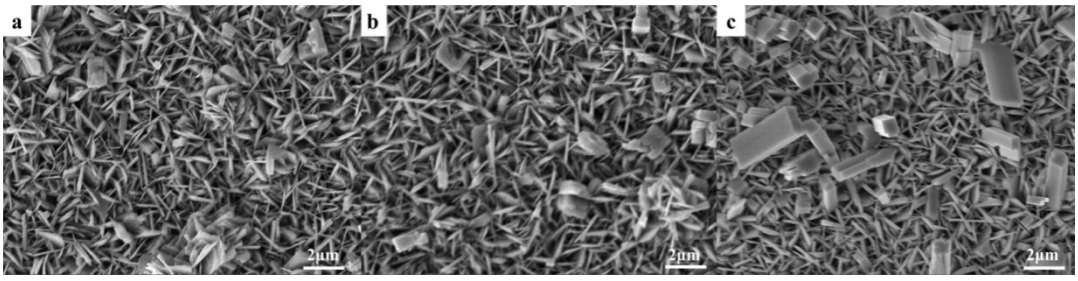

Fig. S1. SEM images of WO_{3-x} synthesized by (a) 180°C, 4 h, (b) 8 h and (c) 36 h.

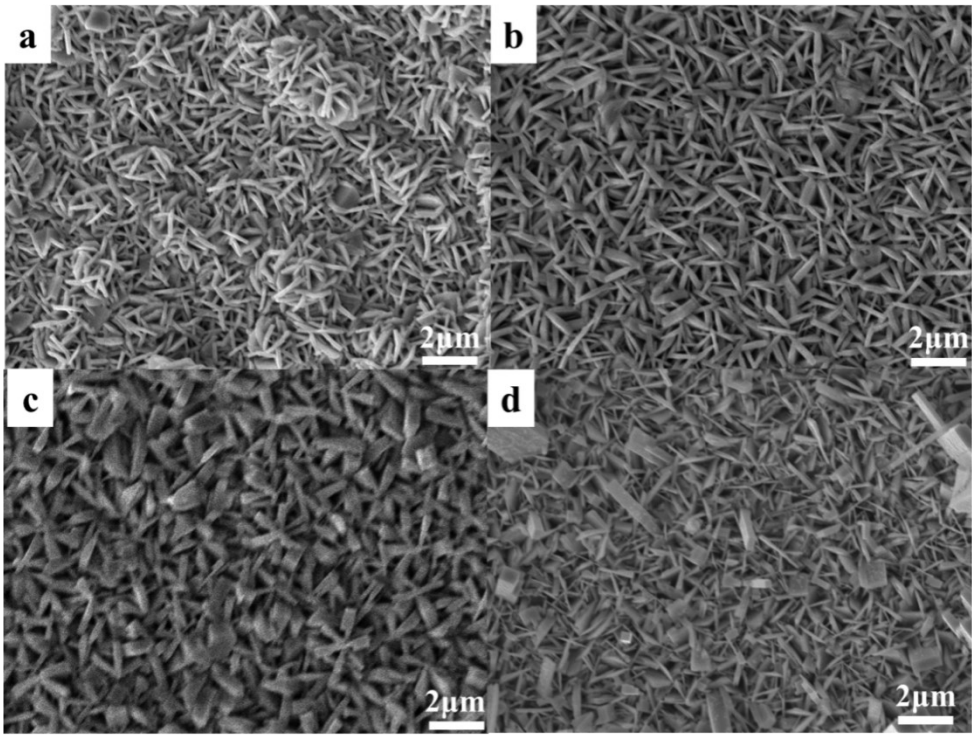

Fig. S2. SEM images of WO_{3-x} synthesized by (a) 120°C, (b) 140°C, (c) 160°C and (d) 200°C.

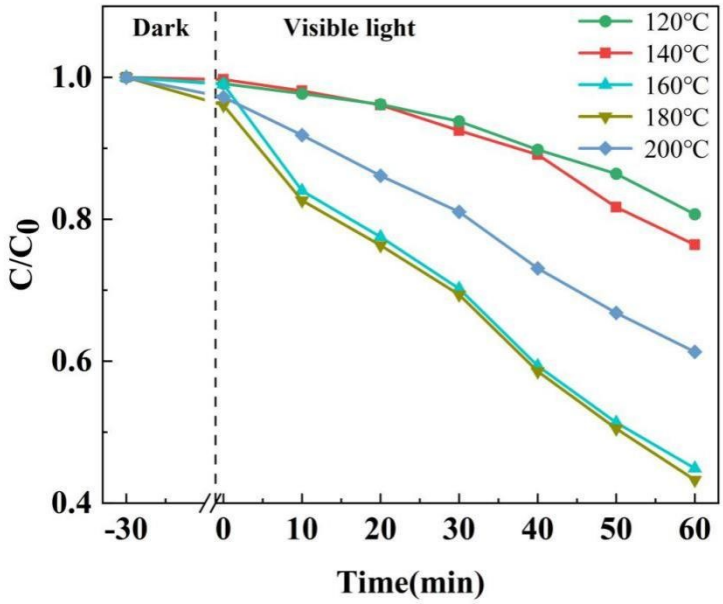

Fig. S3. Comparison of the efficiency of WO_{3-x} catalysts synthesized at different temperatures for degradation of MB.

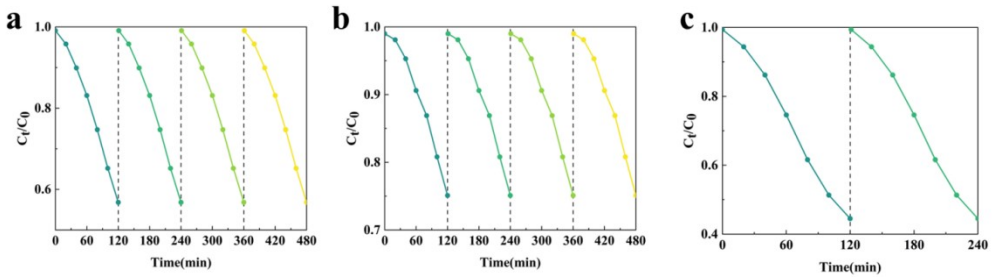

Fig. S4. The stability of WO_{3-x} synthesized by 180°C (a) 4 h, (b) 8 h and (c) 36 h.

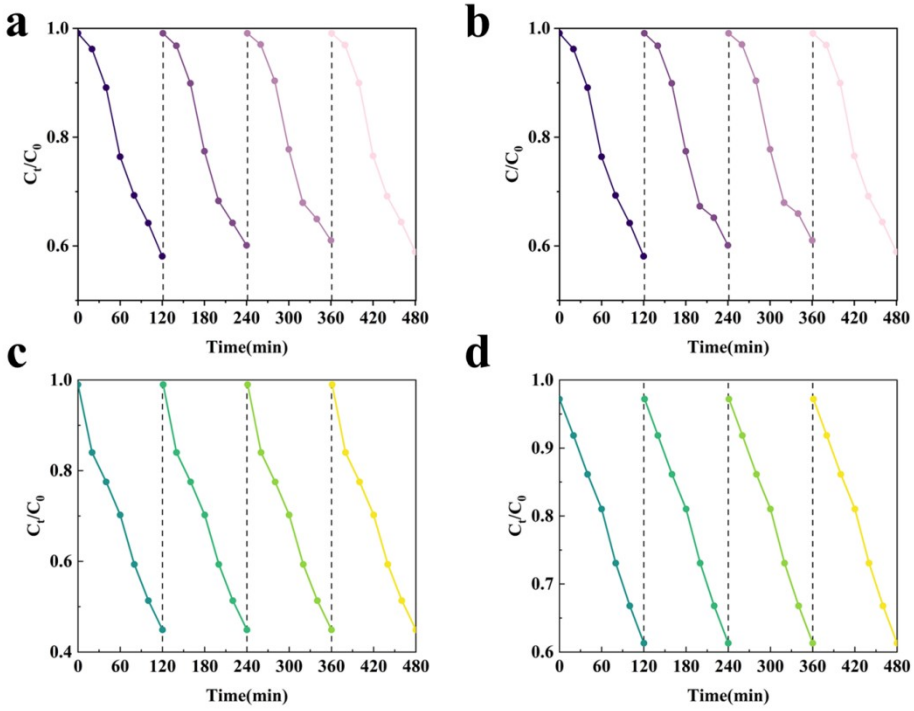

Fig. S5. The stability of WO_{3-x} synthesized by (a) 120°C, (b) 140°C, (c) 160°C and (d) 200°C.

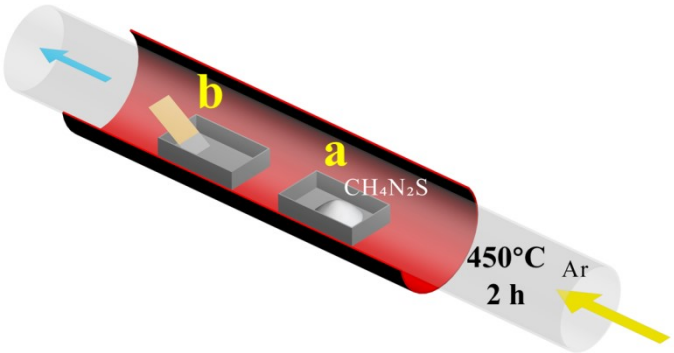

Fig. S6. Schematic diagram of in-situ sulfurization.

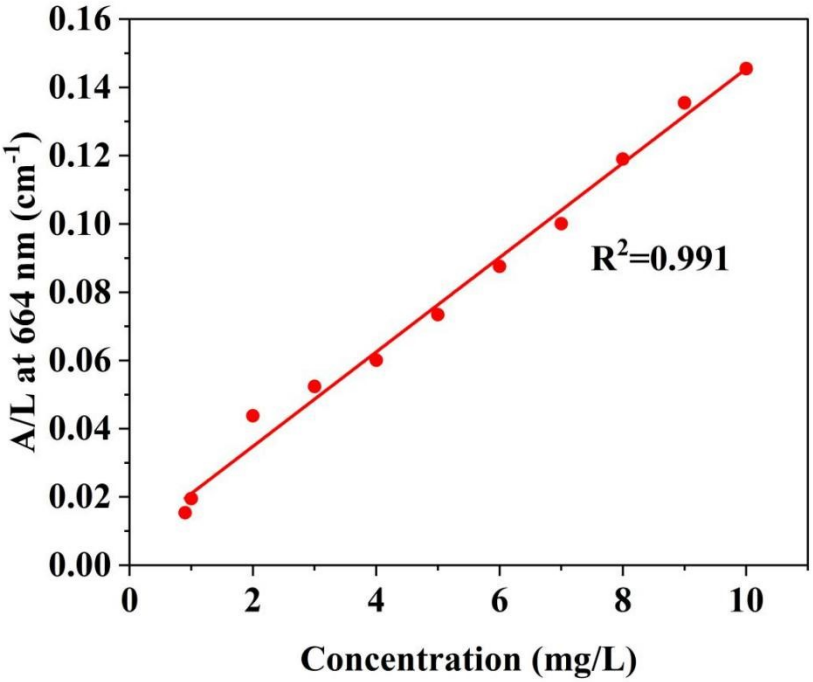

Fig. S7. The absorbance standard curve of MB.

Firstly, the curve of standard MB was determined. Weigh 10 mg of MB and add it to 1000 ml of water, stir well to get 10 mg $L^{-1}$of MB solution. Then the solution of 1-9 mg L^{-1} was obtained by taking samples of methylene blue and diluting them respectively. The absorbance at 664 nm was measured by UV-visible photometer and the corresponding primary curve was made. As shown in Fig. S7, there was a linear relationship between absorbance and concentration and R^2=0.991, which proved that there was a linear relationship between the two.

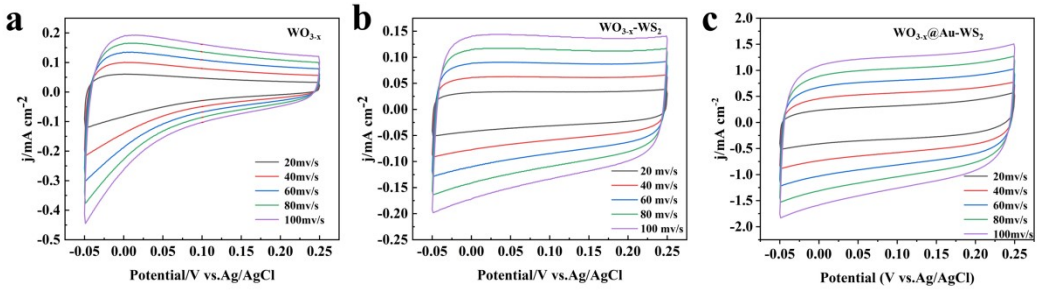

Fig. S8. CV curves of (a) WO_{3-x}, (b) WO_{3-x}-WS_2 and (c) WO_{3-x}@Au-WS_2.

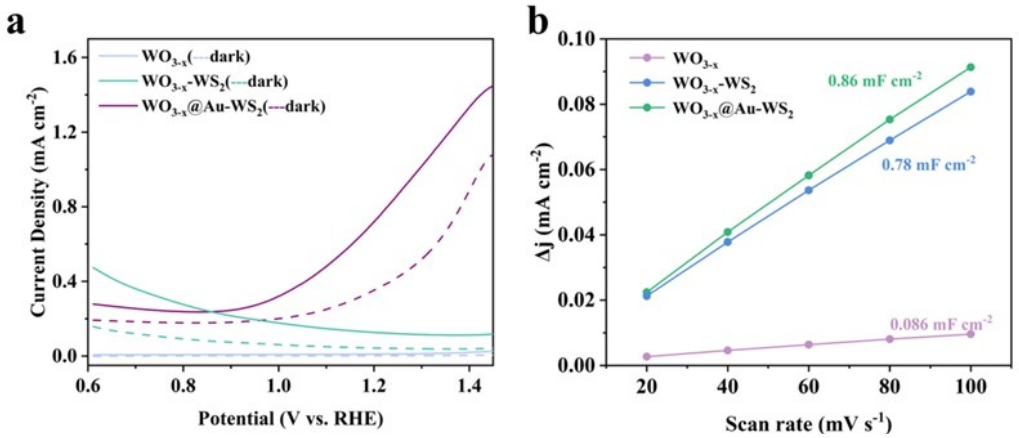

Fig. S9. (a) LSV curves of WO_{3-x}, WO_{3-x}-WS_2 and WO_{3-x}@Au-WS_2; (b) ECSA for WO_{3-x}, WO_{3-x}-WS_2 and WO_{3-x}@Au-WS_2.

According to the LSV data (Fig. S9a), it can be seen that the catalyst photogenerated electrons increase after the addition of light, while the photocurrent decreases without the addition of light, which clearly concludes that the prepared catalysts have a greater proportion of photocatalysis in the photoelectrocatalytic process, whereas electrocatalysis plays the role of applying an electric field for the carrier mobility to play a promotional role only. Tested according to cv (Fig. S9b), the C_{dl} values for WO_{3-x}, WO_{3-x}-WS_2 and WO_{3-x}@Au-WS_2 were determined to be 0.09 mF cm^{-1}, 0.78 mF cm^{-1}, and 0.86 mF cm^{-1}, respectively. The enhanced catalytic degradation performance of the ternary composite can be attributed to its largest electrochemically active surface area (ECSA), which provides abundant active sites for redox reactions.

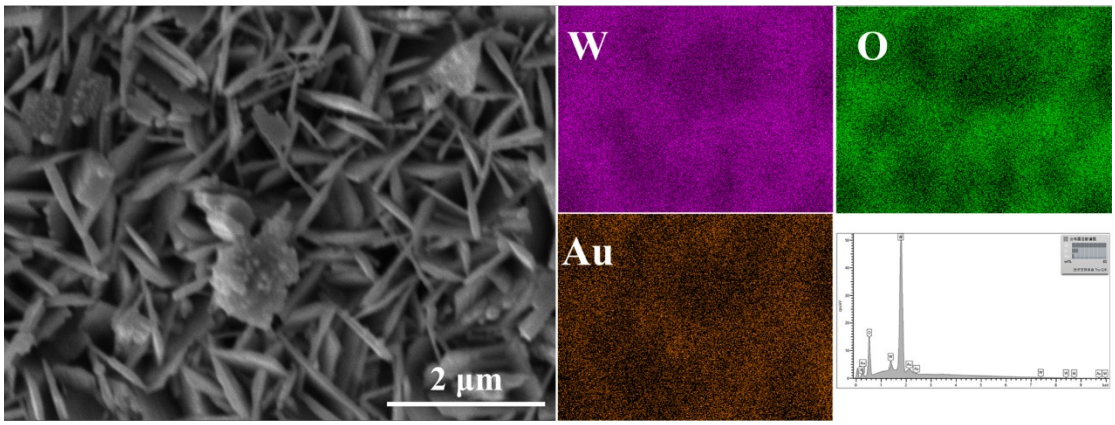

Fig. S10. SEM and EDS images of WO_{3-x}@Au.

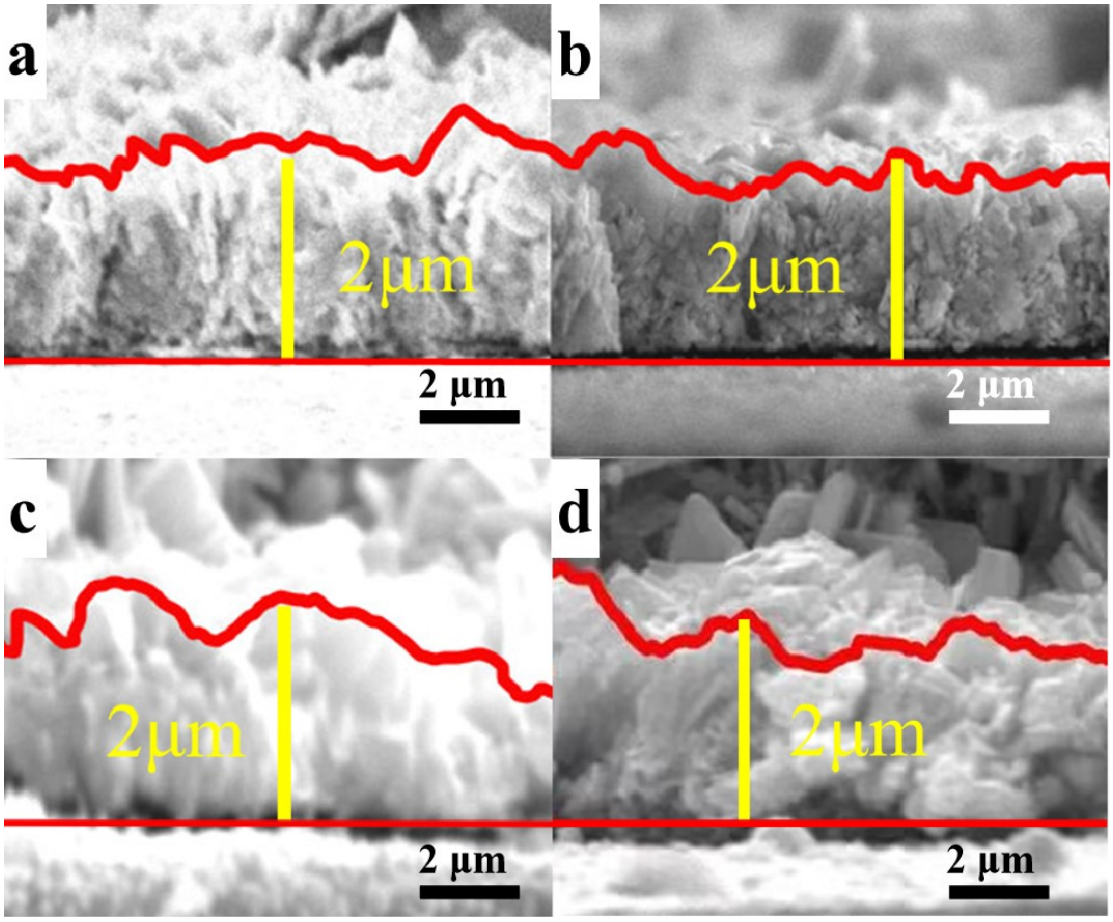

Fig. S11. Thickness of prepared (a) WO_{3-x}, (b) WO_{3-x}-WS_2, WO_{3-x}@Au and WO_{3-x}@Au-WS_2.

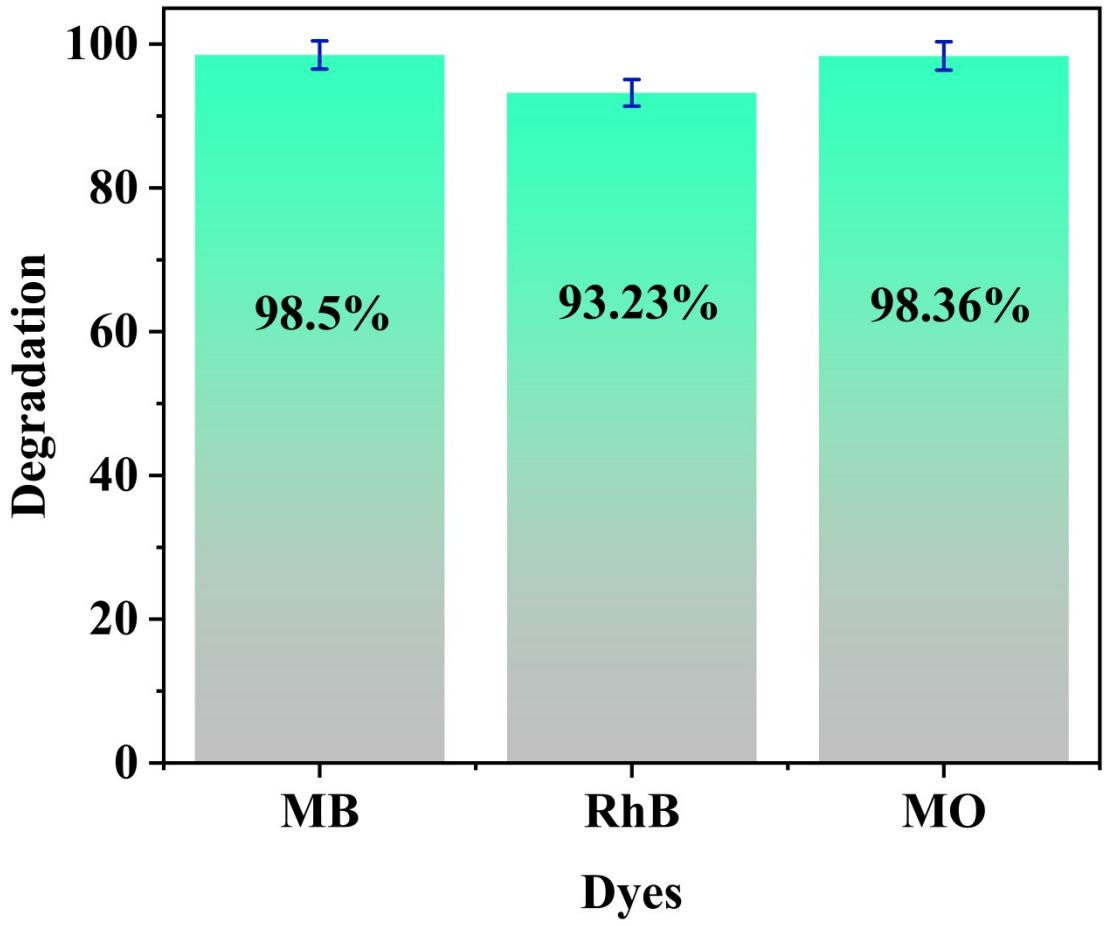

169

170 **Fig. S12.** Comparison of the degradation efficiency for different pollutants.

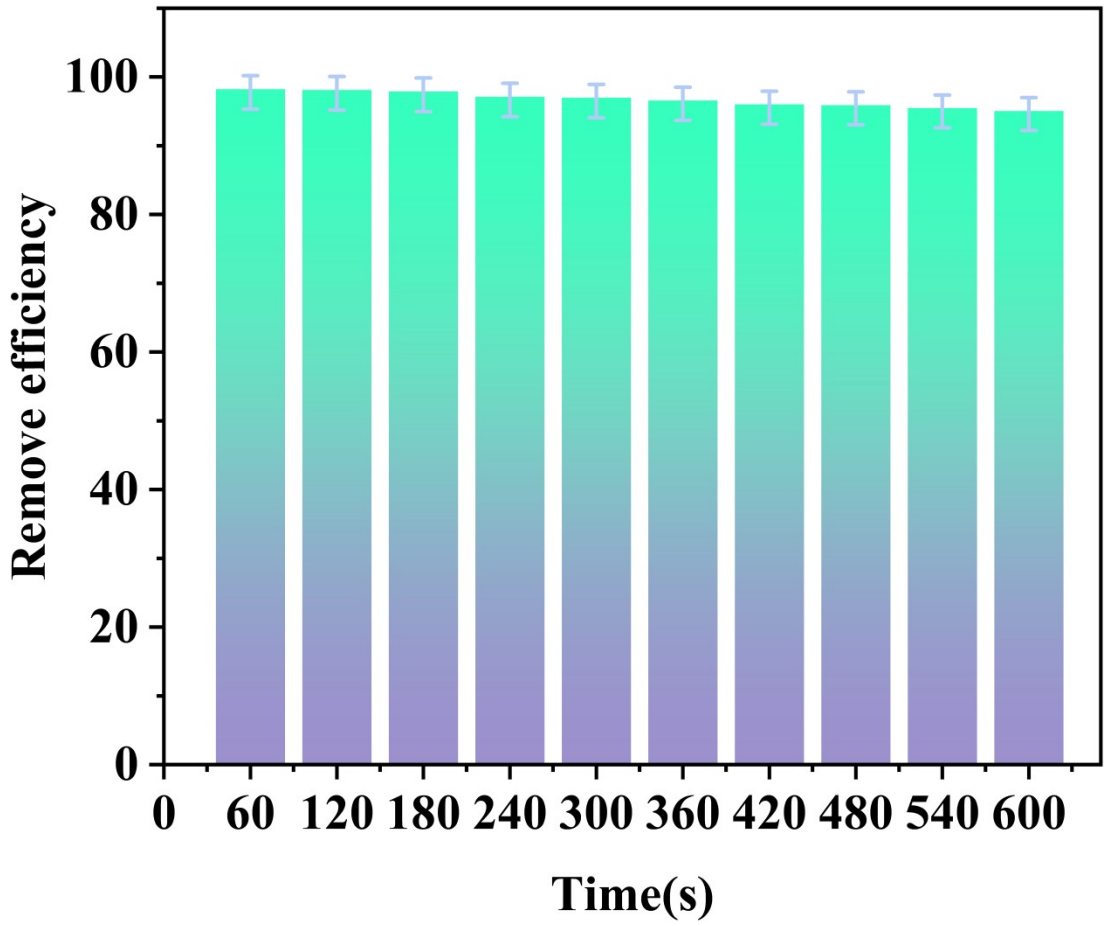

Fig. S13. Degradation of MB after ten consecutive cycles.

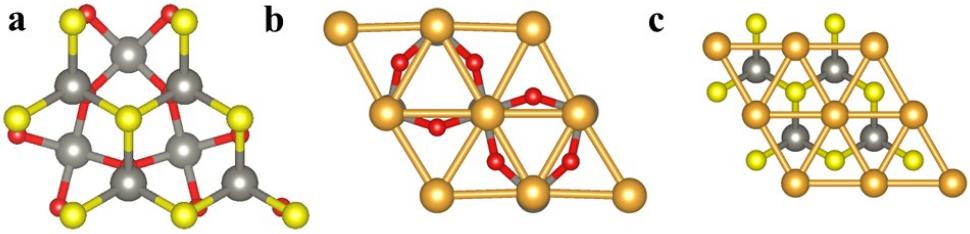

Fig. S14. The cell diagrams of (a) WO_{3-x}-WS_2, (b) WS_2-Au and (c) WO_{3-x}@Au.

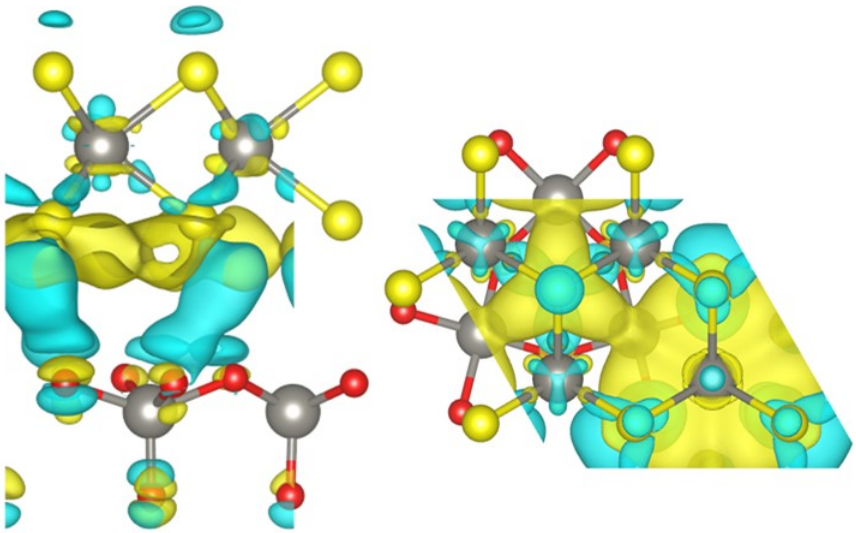

Fig. S15. Side and top views of the charge density difference of WO_{3-x}-WS_2.

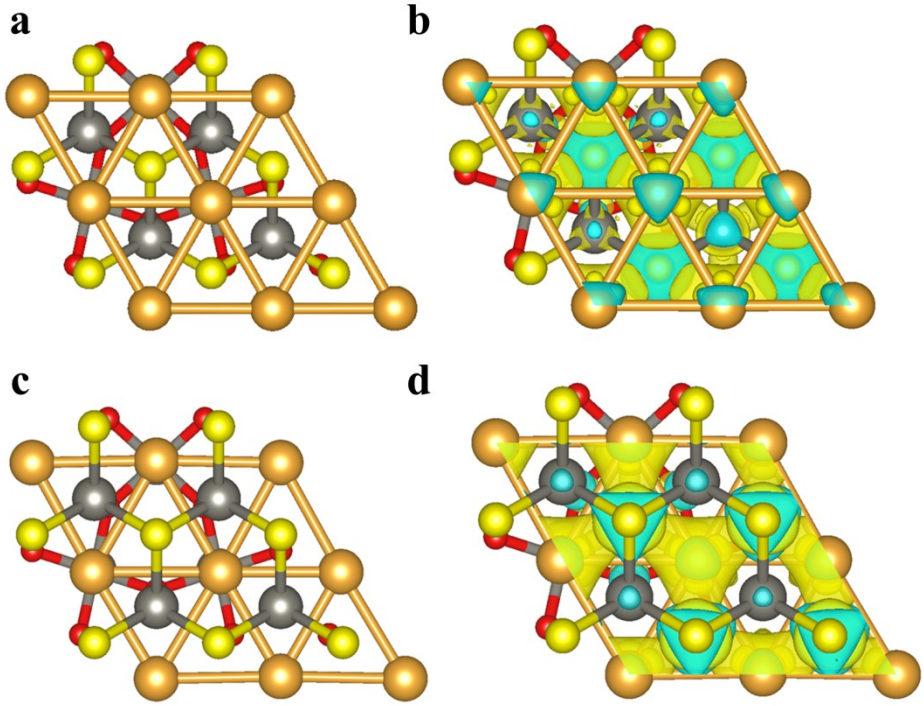

Fig. S16. The cell diagrams and top views of the charge density difference of (a, b) WO_{3-x}-WS_2@Au and (c, d) WO_{3-x}@Au-WS_2.

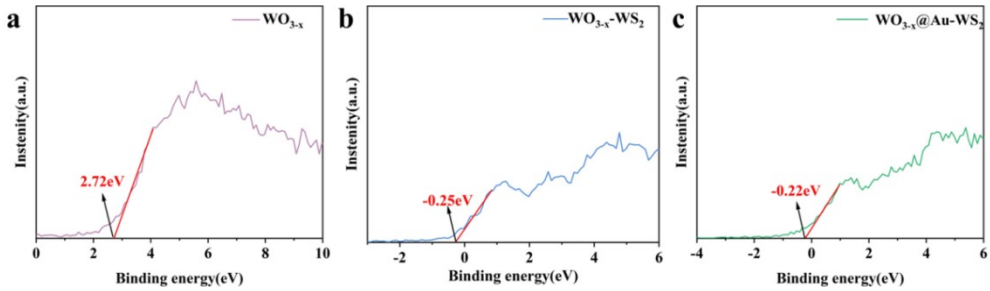

Fig. S17. VB XPS spectra of (a) WO_{3-x}, (b) WO_{3-x}-WS_2 and (c) WO_{3-x}@Au-WS_2.

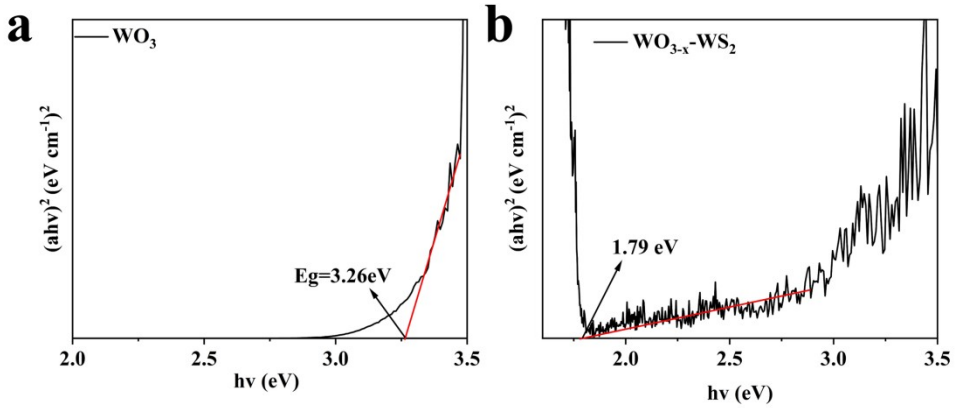

Fig. S18. Tauc's plot of (a) WO_{3-x}, (b) WO_{3-x}-WS_2.

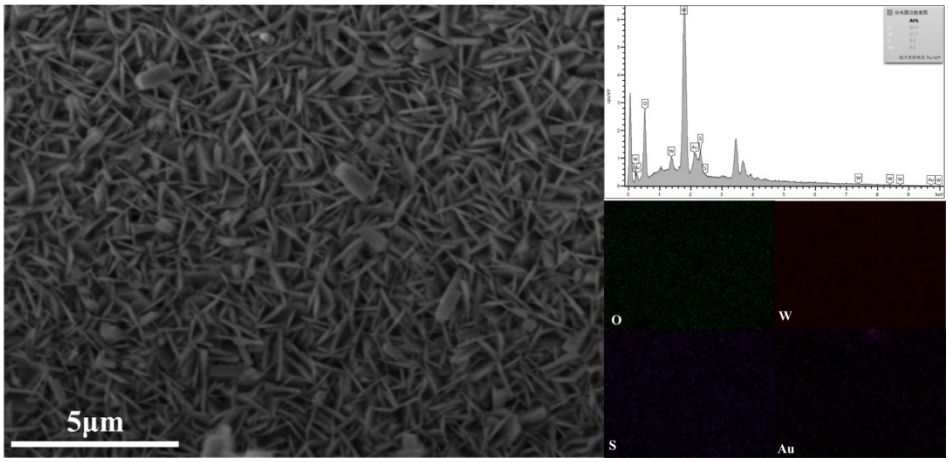

Fig. S19. SEM and EDS images of WO_{3-x}@Au-WS_2.

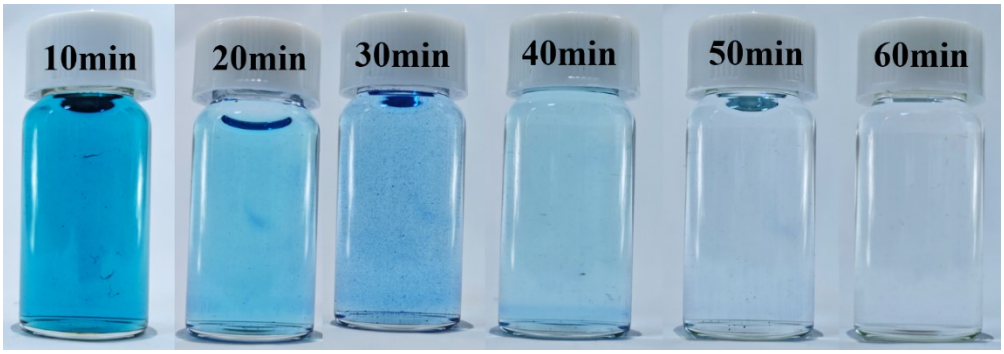

Fig. S20. Visual comparison of (MB) degradation

Catalyst	Degraded substance	Degradation time/min	Remove efficiency/%	Ref
WO_3/Au/FeOOH	Tetracycline hydrochloride	50	99	1
WO_3	TC	90	99	2
hm-m-WO_3/W	BPA	120	99	3
hm-m-WO_3/W	TOC	120	84.5	3
Bi_2MoO_6/WO_3	RhB	240	80.1	4
BiOI-WO_3	3-CP	90-	91.1	5
CQDs/WO_3/TiO_2	BPA	120	75.66	6
TiO_2-NT/WO_3	PPB	30	99	7
WO_3/TiO_2	BA	320	66	8
WO_3	the brilliant blue	240	92	9

WO_3/W	TC	60	90	10
WO_3/$BiVO_4$	MB	180	94	11
s-i-WO_3	BPA	300	93.7	12
CoOOH/WO_3	4-FP	150	99.9	13
Bi_2O_3-WO_3	NOR	360	88.4	14
CuO-Cu_2O/WO_3	DON	180	87.6	15
This work	MB	60	98.5	

188 **Table. S1** Degradation efficiency of pollutants by different WO_3-based catalysts.

Catalysts	The first degradation	The second degradation	The third degradation	Mean ± standard deviation
WO_{3-x}	55.21%	57.93%	57.12%	56.72%±1.31%
WO_{3-x}-WS_2	78.95%	81.23%	80.42%	80.20%±1.14%
WO_{3-x}@Au–WS_2	97.85%	99.12%	98.6%	98.52%±0.63%

189 **Table. S2** Three times of pollutants Degradation by WO_{3-x}, WO_{3-x}-WS_2 and WO_{3-x}@Au–WS_2.

Catalyst	Degraded substance	Degradation method	Degradation time/min	Remove efficiency/ %	Ref
WO_3	MB	PEC	120min	98.56%	16
WS_2	MB	photocatalysis	180min	67.6%	17
WS_2	MB	photocatalysis	80min	41.86%	18
WO_{3-x}	MB	PEC	60min	55.1%	This work

190 **Table. S3** Degradation efficiency of pollutants by individual WO_3 and WS_2.

References

1. J. Wang, L. Jiang, F. Liu, M. Jia, M. Liu, J. Li and Y. Lai, *Chemical engineering journal*, 2021, **407**, 127195.
2. B. A. Koiki and O. A. Arotiba, *Heliyon*, 2023, **9**.
3. Q. Ma, R. Song, F. Ren, H. Wang, W. Gao, Z. Li and C. Li, *Applied Catalysis B: Environmental*, 2022, **309**, 121292.
4. Z. Zhang, C. Zhao, S. Lin, H. Li, Y. Feng and X. Gao, *Fuel*, 2021, **285**, 119171.
5. S. Li, J. Liu, X. Liu, K. Yan and J. Zhang, *Electrochimica Acta*, 2024, **484**, 144058.
6. Z. Liang, X. Zhang, J. Yang, Y. Cheng, H. Hou, S. Hussain, J. Liu, G. Qiao and G. Liu, *Journal of Hazardous Materials*, 2023, **443**, 130316.
7. A. S. Martins, L. Nunez and M. R. d. V. Lanza, *Journal of Electroanalytical Chemistry*, 2017, **802**, 33–39.
8. Y. M. Hunge, *Ceramics International*, 2017, **43**, 10089–10096.
9. Y. Hunge, A. Yadav, M. Mahadik, V. Mathe and C. Bhosale, *Journal of the Taiwan Institute of Chemical Engineers*, 2018, **85**, 273–281.
10. A. S. Martins, T. T. Guaraldo, J. Wenk, D. Mattia and M. V. B. Zanoni, *Journal of Electroanalytical Chemistry*, 2022, **920**, 116617.
11. W. Nareejun and C. Ponchio, *Solar energy materials and solar cells*, 2020, **212**, 110556.
12. W.-K. Wang, L.-L. Zhou, H.-Y. Cao, P.-X. Liu, X.-Y. Li, M. Fujitsuka, J. Xu and T. Majima, *Applied Surface Science*, 2023, **618**, 156686.
13. Q. Ma, Z. Ning, M. Fang, G. Zhang, H. Guo, J. Zhou and T. Wang, *Chemical Engineering Journal*, 2024, **498**, 155551.
14. T. Jiang, L. Cheng, Y. Han, J. Feng and J. Zhang, *Separation and Purification Technology*, 2020, **238**, 116428.
15. L. Cheng, T. Jiang and J. Zhang, *Science of the Total Environment*, 2021, **776**, 145840.
16. Y. Hunge, M. Mahadik, V. Mohite, S. Kumbhar, N. Deshpande, K. Rajpure, A. Moholkar, P. Patil and C. Bhosale, *Journal of Materials Science: Materials in Electronics*, 2016, **27**, 1629–1635.
17. M. Al Qaydi, N. S. Rajput, M. Lejeune, A. Bouchalkha, M. El Marssi, S. Cordette, C. Kasmi and M. Jouiad, *Beilstein Journal of Nanotechnology*, 2024, **15**, 817–829.
18. V. Shinde, P. Tanwade, T. Katayama, A. Furube, B. Sathe and P. Koinkar, *Surfaces and Interfaces*, 2024, **46**, 104067.